

**EXPERIMENTAL STUDIES IN PLATE HEAT EXCHANGER USING  
THERMINOL-55 /Al<sub>2</sub>O<sub>3</sub> & GLYCEROL/Al<sub>2</sub>O<sub>3</sub> NANOFLUIDS**

Periasamy Manikandan Srinivasan<sup>1\*</sup>, Nesakumar Dharmakkan

Department of Chemical Engineering, Kongu Engineering College, Erode-638 060, India

<https://doi.org/10.2298/CICEQ240903035S>

**Received 3.09.2024.**

**Revised 3.11.2024**

**Accepted 22.11.2024**

---

<sup>1</sup> Corresponding Author: Periasamy Manikandan Srinivasan, Tel: 91-4294-226426,09442520334; e-

mail:[sriperiasamy@gmail.com](mailto:sriperiasamy@gmail.com)

**Abstract:** The experiment aimed to compare the heat transfer performance of two base fluids, Therminol-55 and Glycerol, both mixed with aluminium oxide nanoparticle. The investigation focused on assessing how the addition of aluminium oxide nanoparticles (at concentrations of 0.1%, 0.2%, and 0.25% by volume) affected heat transfer in a plate heat exchanger using a mixture of Therminol-55/water and Glycerol/water. Results demonstrated a significant enhancement in heat transfer efficiency for both hot and cold sides of the exchanger when using these nanoparticle-infused base fluid mixtures. Specifically, the study observed notably improved heat transfer coefficients for the Therminol-55/water mixture with a 0.25% nanoparticle concentration, achieving 3858.77 W/m<sup>2</sup>K (23% higher) for the hot fluid coefficient, 4194.54 W/m<sup>2</sup>K (31% higher) for the cold fluid coefficient, and an overall coefficient of 2310 W/m<sup>2</sup>K (23% higher) . Similarly, the Glycerol/water mixture with a 0.25% nanoparticle concentration exhibited superior performance, reaching 4491.23 W/m<sup>2</sup>K (30% higher) for the hot fluid coefficient, 4394.54 W/m<sup>2</sup>K (35.5% higher)for the cold fluid coefficient, and an overall coefficient of 2508 W/m<sup>2</sup>K (27.8% higher). These findings indicate that the Glycerol/water mixture with aluminium oxide nanoparticles outperforms the Therminol-55/water counterpart, suggesting its potential to minimize temperature differentials within the heat exchanger and enhance operational effectiveness.

**Keywords:** Al<sub>2</sub>O<sub>3</sub>, heat transfer, therminol-55, glycerol, nano fluid, plate heat exchanger.

### **Article Highlights**

- Al<sub>2</sub>O<sub>3</sub>/Therminol-55/ Water and Al<sub>2</sub>O<sub>3</sub>/Glycerol/ Water mixed nanofluid were prepared
- Heat transfer performance of Al<sub>2</sub>O<sub>3</sub> suspended base fluid was studied in a plate heat exchanger
- Individual and overall heat transfer coefficient were determined and analyzed by varying flow rate

## Introduction

Nanoparticles are particles less than 100 nm in size[1]. Both synthetic and naturally occurring nanoparticles can be found in the environment. Inorganic substances are called nanoparticles. Nanoparticles are invisible to the naked eye. They can be divided into several categories according to their sizes, forms, and features. The large surface area and nanoscale size of nanoparticles give them distinct physical and chemical characteristics. Their distinct composition, size, and form greatly influence their toughness, reactivity, and other qualities. These tiny particles are ideal for strong chemical reactivity, bio mobility, and energy absorption because of their unique properties. Nanomaterials are divided into four categories: 0D, 1D, 2D, and 3D, depending on their general form[2]. At least one dimension of nanoclusters is between 1 and 10 nm in size, exhibiting a small size distribution. Heat exchangers are used in industrial production processes to warm and cool fluids [3,4]. Glycols/aluminum oxide nanofluid used as a base fluid in heat transfer applications. To achieve better heat transfer, we need to focus on improving the thermal conductivity and overall heat transfer characteristics of these fluids [5-8].

Recent advancements in energy reduction through the use of nanofluids are evident in a substantial body of research within the technical community. This innovative engineering fluid, known for its specialized applications, has the capability to lower costs in heat transfer operations by modifying appropriate base fluids [9]. Researchers have developed heat transfer fluids containing suspended nanoparticles for various heat transfer equipment [10,11]. Numerous researchers employed various metal oxides, including the addition of CuO nanoparticles to water[12,13], aluminium oxide/water[14], aluminium oxide/water-methanol [15], graphene/water-glycol[16], TiO<sub>2</sub>, ZnO in water-ethylene glycol[17], Fe<sub>2</sub>O<sub>3</sub> in engine oil-water mixture, Al<sub>2</sub>O<sub>3</sub> and CuO nanoparticle suspension in engine oil, vacuum pump fluid, distilled water and ethylene glycol[18] and the results showed that this addition considerably increases the thermal conductivities of fluid mixtures and heat transfer coefficient. In experimental results of Al<sub>2</sub>O<sub>3</sub> nanoparticle addition shows that the Nusselt number increased significantly with respect to different and volume fraction [19]. This study investigates the use of nanofluids for enhanced heat transfer in the oil and gas industry. Therminol 66, a common heat transfer fluid in heat exchangers, was chosen as the base fluid. To improve its heat transfer capabilities, Iron oxide (III) nanoparticles were incorporated at a concentration of 0.3% by weight (wt%). The fundamental properties of these nanofluids, such as density, viscosity, and specific heat capacity, were then measured as the heat transfer increased up to 46%, pressure drop increased up to 37.5% and friction factor increased up to 10% [20]. Result of the heat transfer effect showed energy savings of around 32% for cooling. Methanol is recently used for

variety of heat transfer applications and different type of heat pipes (vapor–dynamic thermosyphons, conventional and micro heat pipe).

Numerous research works have looked into the special qualities and abilities these novel fluids have shown since nanofluids were first used in a variety of industries. The economically feasible nanomaterial aluminum oxide ( $\text{Al}_2\text{O}_3$ ) has good thermophysical and heat transport properties and is non-toxic [21]. Heat transfer study was performed in Armfield plate heat exchanger (HT32) with an Armfield heat exchange service unit (HT30X) by preparing suspension of multi-wall carbon nanotubes in distilled water Hassaan et al., reported 32% increase in Nusselt number (with 1.53% volume fraction) and with the same nanofluids in Shell and tube heat exchanger the percentage increase of the overall heat coefficient ranges between 6% and 76.4%, compared to distilled water [22, 23] was reported. Heat transfer performance of two distinct heat exchangers with the same heat transfer area was assessed by Hassaan et al., with a tubular heat exchanger (THE) and a shell-and-tube heat exchanger (STHE) and obtained heat transfer coefficient of STHE is 7–43% greater than that of tubular heat exchanger [24], also proposed a relationship between Reynolds number and MWCNT volume concentration for computing the Nusselt number [25]. In a plate heat exchangers (PHEs) hybrid nanofluid (multi-walled carbon nanotubes (MWCNTs)– $\text{Al}_2\text{O}_3$ /water) was used with various concentrations and reported increase in the overall heat coefficient from 6% to 97% compared to pure distilled water [26]. Experiment was done using MWCNTs as operating fluids in an automotive radiator with louvered fins and flat tubes (Honda Civic 2005). From the study they reported Nusselt number increment of 13.72% in comparison to pure water, also a correlation for estimating the Nusselt number in terms of the Reynolds number and MWCNTs volume concentration is provided [27]. While most research on the topic focuses on thermal conductivity studies, there is potential to investigate this material's heat transfer capabilities in real-time heat exchangers. Although employing nanofluids has many advantages, there are some disadvantages as well, such as instability, fouling, and surface erosion [28 - 30]. Therminol-55 provides a method to resist fouling, decreasing pressure drop, increase heat transfer in ribbed tube and stop nanoparticle aggregation when making a nanofluid. Since the literature also demonstrates the effectiveness of small plate heat exchangers, we decided to use them in our inquiry [31]. Prior research hasn't explored the heat transfer performance of a specific nanofluid mixture:  $\text{Al}_2\text{O}_3$ -Water-Therminol-55 (AWT) within plate heat exchangers [32]. Also it was found that  $\text{Al}_2\text{O}_3$  Nanoparticle containing Nanofluids shown increased critical heat flux, which was due to the improved Thermal conductivity of nanoparticles [34], hence  $\text{Al}_2\text{O}_3$  was chosen. Elaboration of significant factors that play a vital part in enhancing heat transfer characteristics of nanofluid is

also needed to explore the heat transfer performance of nanofluids [35]. To address this gap, we investigated how adding Al<sub>2</sub>O<sub>3</sub> nanoparticles (0.1% to 0.25% concentration) affects heat transfer in a Therminol-55/Water and Glycerol/water base fluid (5:95 volume ratio). The experiments were conducted at a constant hot fluid inlet temperature (60°C) with varying flow rates (2 to 6 liters per minute).

## Materials and Methods

### Preparation and Properties of nanoparticle

Nano powders refer to agglomerates of ultrafine particles, nanoparticles, or Nano clusters. Nano particles consist of three layers—surface layer, shell layer, and core layer. From the literature it was noticed that To obtain stable Al<sub>2</sub>O<sub>3</sub> nanofluids, many routes exist such as surfactant addition, pH control, ultrasonic agitation, functionalization, magnetic stirring, and high-pressure homogenization [36]. Hence in this study, conversion of nanoparticles into Nano fluids is achieved through a two-step method with the help of high-pressure homogenizer. The conversion of nanoparticles into Nano fluids is achieved through a two-step method. In this research, a two-step (sol-gel) technique was employed to suspend 50 nm Al<sub>2</sub>O<sub>3</sub> nanoparticles in a water-methanol mixture. Base fluids with specific volume fractions (5% Therminol-55 + 95% water) were formulated according to calculated amounts derived from the below fraction Equation (1).

$$\phi = \frac{\left(\frac{m}{\rho}\right)_{Al_2O_3}}{\left(\frac{m}{\rho}\right)_{Al_2O_3} + \left(\frac{m}{\rho}\right)_{W:T}} \quad (1)$$

To ensure stability in the prepared nanofluid, a high-pressure homogenizer was employed, and the resulting nanofluid served as the cold fluid in the plate heat exchanger. The utilization of a high-pressure homogenizer ensures the uniform suspension of the prepared nanofluid throughout the base fluid. When designing energy-efficient systems, the thermal conductivity of heating or cooling fluids plays a crucial role. Among the key considerations in developing and controlling the process is the fluid's ability to conduct heat. Factors such as availability, cost, heat conductance, and the propensity of particles to stay uniformly dispersed in the base fluid with minimal agglomeration are all significant. Despite their superior thermal conductivity,

metal oxide nanoparticles tend to agglomerate. In our investigation, we used Aluminum oxide ( $\text{Al}_2\text{O}_3$ ) nanofluid for heat transfer analysis.

### **SEM Images of Aluminium oxide nanoparticle**

Widely employed for material analysis, SEM (Scanning Electron Microscopy) plays a crucial role in identifying the microstructure and chemistry of materials. By projecting and scanning a focused stream of electrons across the surface, SEM produces detailed images. The interaction of electrons in the beam with the sample generates various signals, providing valuable information about the surface's composition. Figure 1 depicts SEM images of  $\text{Al}_2\text{O}_3$  nanoparticles.

**Figure 1**

### **Experimental Setup and Estimation of thermo physical properties:**

Experiments were conducted on a plate-type heat exchanger as described in the experimental setup (Schematic and photographic view) illustrated in Figure 2. Plate heat exchanger consists of 13 Stainless Steel corrugated plates (Alfa Laval, India) providing seven flow channels for the hot fluid and six flow channels for the cold fluid. The plate length and thickness of the plate are 0.154m and 0.25mm respectively.

Thermal conductivity was measured using thermal conductivity analyzer (Scientico, India) and viscosity was measured with redwood viscometer for all the concentrations of nanofluid.

Density of nanofluid and specific heat capacity of nanofluid are calculated from the correlations [36, 37] given in the equations (2) and (3).

$$\rho_{nf} = (1 - \phi)\rho_f + \phi\rho_p \quad (2)$$

$$C_{p,nf} = ((1 - \phi)\rho_f C_{pf} + \phi\rho_p C_{pp}) / (\rho_{nf}) \quad (3)$$

Obtained results of thermophysical properties were used for calculating different dimensionless numbers (Reynolds, Prandtl and Nusselt number) applied in this study.

Nanofluids based on Therminol-55 incorporating  $\text{Al}_2\text{O}_3$  nanoparticles were prepared at different volume concentrations, including 0.1%, 0.2%, and 0.25%. The density, dynamic viscosity, heating value, and heat conductivity were subsequently calculated based on experimental findings.

**Figure 2**

### **Determination of Nusselt number, convective and overall heat transfer coefficient of $\text{Al}_2\text{O}_3$ /Water-Methanol nanofluid:**

### **Determination of thermophysical properties of Fe<sub>2</sub>O<sub>3</sub>-Water-Engine Oil nanofluid:**

Equation (2), based on the Kim model, is employed to calculate the Nusselt number of the nanofluid. Equation (3) is utilized to determine the heat transfer coefficient of both the hot and cold fluids. Equation (4) is employed to find the overall heat transfer coefficient.

$$Nu = 0.295(N_{Re})^{0.64} (N_{Pr})^{0.32} ((\Pi/2) - \beta) \quad (4)$$

$$h = \left( \frac{(Nu)(D_H)}{K} \right) \quad (5)$$

$$U = \left( \frac{(Q)_{avg}}{(A)(\Delta T_{lmtl})} \right) \quad (6)$$

### **Results and Discussion**

#### **Effect of flow rate on hot fluid heat transfer coefficient( $h_h$ ) for Therminol-55/Water base fluid at 60°C:**

Prior to conducting in-depth experiments with chosen nanofluids, a preliminary study was carried out using de-ionized water to ensure the experimental study's reliability. Figure 3 illustrates the impact of flow rate on the heat transfer coefficient ( $h_h$ ) of the hot fluid at a hot fluid inlet temperature of 60°C, considering various nanofluid concentrations (Therminol-55&Al<sub>2</sub>O<sub>3</sub>) and water.

#### **Figure 3**

According to the Figure 3, The heat transfer coefficient on the hot side ( $h_h$ ) ranges from 1980 W/m<sup>2</sup>K for water-water, increasing to 2620 W/m<sup>2</sup>K at a flow rate of 2 lpm for a nanofluid with a nanoparticle concentration of 0.25. With an increase in flow rate to 6 lpm, the heat transfer coefficient range also expands, starting at 3145 W/m<sup>2</sup>K for water-water and rising to 3858.77 W/m<sup>2</sup>K (for 0.25 vol.%). This underscores the significant impact of flow rate on enhancing heat transfer. This increment is due to the fact that there is a significant increment in Reynolds number because of the incremental effect in density with respect to viscosity of a nanofluid. Because of Reynolds number increment and thermal capacity, rate of heat transfer increasing significantly.

#### **Effect of flow rate on cold fluid heat transfer coefficient( $h_c$ ) for Therminol-55/Water base fluid at 60°C:**

The effects of varying flow rates on the heat transfer coefficient on the cold side at 60°C for Therminol-55/Water base fluid was investigated and are depicted in Figure 4.

#### Figure 4

A consistent upward trend in heat transfer enhancement is evident on the cold side fluid, as depicted in Figure 4. Notably, at a low flow rate (2 lpm) and a low nanoparticle concentration (0.25 vol.%), the heat transfer coefficient closely aligns with that of water as the base fluid. However, a gradual increase in the flow rate leads to a corresponding increase in the heat transfer rate. For example, at a flow rate of 4 lpm, the heat transfer coefficient rose to 2908.82 W/m<sup>2</sup>K (for 0.25 vol.%) from 2435.76 W/m<sup>2</sup>K (for water).

The results indicate that both the convective heat transfer coefficient and Nusselt number for Al<sub>2</sub>O<sub>3</sub>/Therminol-55-water nanofluid surpass those of the base fluid. This enhancement is attributed to the improved heat transport facilitated by thermally conductive nanoparticles through the interfacial layers of fluids. The maximum enhancement was observed at 6 lpm, with a heat transfer coefficient value of 4194.54 W/m<sup>2</sup>K (for 0.25 vol.); however, the rate of enhancement diminishes with increasing flow rate. Hence, optimizing the flow rate is essential for the efficient utilization of nanoparticles.

#### **Effect of flow rate on hot fluid heat transfer coefficient( $h_h$ ) for Glycerol/Water base fluid at 60°C:**

Given the significant impact of base fluid on heat transfer, the study was replicated with alterations in base fluid composition. This included varying the concentration and observing the effect of flow rate on the heat transfer coefficient of the hot fluid for glycerol/water-based fluid as depicted in Figure 5.

#### Figure 5

According to the data presented in Figure 5, the heat transfer coefficients for various concentrations (ranging from 0.1 vol.% to 0.25 vol.%) show notable differences. At a flow rate of 2 lpm, the heat transfer coefficient on the hot side was recorded at 1992.23 W/m<sup>2</sup>K for water, 3845.17 W/m<sup>2</sup>K for 0.1 vol.%, and 4491.23 W/m<sup>2</sup>K for 0.25 vol.%. Similarly, at a flow rate of 6 lpm, the corresponding values were 3145.89 W/m<sup>2</sup>K for water, 3845.17 W/m<sup>2</sup>K for 0.1 vol.%, and 4101.24 W/m<sup>2</sup>K for 0.25 vol.%. These results once again underscore the effectiveness of nanoparticle suspension in enhancing heat transfer. It is also conformed from Figure 5 that the heat transfer coefficient ( $h_h$ ) enhancement is directly proportional with nanoparticle concentration and flow rate; however the maximum enhancement was noted at 0.25 volume% of nanoparticle volume fraction.

#### **Effect of flow rate on cold fluid heat transfer coefficient( $h_c$ ) for Glycerol/Water base fluid at 60°C:**



The influence of flow rate on the heat transfer coefficient of the cold side at 60°C for the glycerol/water base fluid is depicted in Figure 6.

### **Figure 6**

The impact on the heat transfer coefficient of the cold side demonstrates an increase with a flow rate of 2 LPM, rising from 1466.25 W/m<sup>2</sup>K (for water) to 2331.96 W/m<sup>2</sup>K (for 0.25 vol.% nanoparticle concentration). Similarly, at a flow rate of 6 LPM, the cold side heat transfer coefficient increased from 3356.76 W/m<sup>2</sup>K (for water) to 4394.54 W/m<sup>2</sup>K (for 0.25 vol.% nanoparticle concentration). A notable enhancement in comparison to the Therminol-55/water base fluid was observed. This trend indicates a consistent rise in heat transfer rate, which correlates linearly with both nanoparticle concentration and temperature.

### **Effect of flow rate on overall heat transfer coefficient(U) for Therminol-55/Water and Glycerol/Water base fluid at 60°C:**

While the heat transfer coefficient was initially computed for individual fluids, calculating the overall heat transfer coefficient is crucial to harness the advantages offered by nanoparticles. Therefore, the findings regarding the overall heat transfer coefficient at 60°C for Therminol-55/Water base fluid are illustrated in Figure 7(a).

### **Figure 7**

From Figure 7(a), it is evident that at flow rates of 2, 4, and 6 lpm, the range of U was 673.87, 1285.65, and 1918.41 W/m<sup>2</sup>K (for 0.1 vol. % nanoparticle) and 742.57, 1600, and 2310.92 W/m<sup>2</sup>K (for 0.25 vol. %). This observation leads to the conclusion that both individual and overall heat transfer coefficients were significantly enhanced due to the presence of nano-sized solid particles.

The impact of flow rate variations on the overall heat transfer coefficient at 60°C for the glycerol/water base fluid is illustrated in Figure 7(b). From Figure 7(b), it was noted that the changing the base fluid favors heat transfer; hence study was performed for both the base fluids (Therminol-55/Glycerol). Result shows that uniform enhancement in overall heat transfer rate with respect to all the concentrations (0.1, 0.2 and 0.25 vol. %) and all the flow rates. The ranges were 2118.41 W/m<sup>2</sup>K (for 0.1 vol. % nanoparticle) to 2508.12 W/m<sup>2</sup>K (for 0.25 vol. % nanoparticle concentration) at a flow rate of 6 lpm.

Due to the incremental effect on thermal conductivity of nanofluids heat transport dominates over the momentum transport and hence the Prandtl number decreases at the highest volume fractions of nanofluid. There exists good agreement between the results calculated from this experimental values and the correlation. It was noticed that the calculated Nusselt number

falls within  $\pm 8\%$  and  $\pm 10\%$  deviation when compared with experimental results of (Al<sub>2</sub>O<sub>3</sub>/Glycerol-water) and (Al<sub>2</sub>O<sub>3</sub>/Therminol-55-water) nanofluids respectively. which shows the accuracy of the results of the experiment. Obtained results are consistent with the reported results that thermal conductivity, viscosity and density of the Al<sub>2</sub>O<sub>3</sub> nanofluids are increased with addition of nanoparticle in the base fluid [22- 28].

### **Conclusion**

- The study revealed a significant enhancement in heat transfer when nanoparticles were added in water-water system. This improvement can be attributed to the high thermal conductivity of the solid nanoparticles, which effectively increase the rate of heat transfer within the base fluid.
- By employing the (Al<sub>2</sub>O<sub>3</sub>/Glycerol-water) nanofluid resulted in notably decreased temperature differentials compared to the nanofluid (Al<sub>2</sub>O<sub>3</sub>/Therminol-55-water) within the heat exchanger, leading to improved performance of the heat exchanger.
- The highest coefficients were observed at 0.25% in Glycerol base fluid and a flow rate of 6 liters per minute (lpm). These peak values comprised a hot fluid coefficient of 4101.24 W/m<sup>2</sup>K, a cold fluid coefficient and an overall coefficient of of 4394.54 W/m<sup>2</sup>K and 2508.12 W/m<sup>2</sup>K respectively.
- Comparing the previously mentioned heat transfer coefficient values of Glycerol base fluid nanoparticle with those of Therminol-55 base fluid nanoparticle reveals that the hot fluid coefficient increases by up to 6.28%, the cold fluid coefficient by up to 4.76%, and the overall coefficient by up to 8.5%.
- Glycerol base fluid nanoparticle has the better heat transfer co-efficient compared to the Therminol-55. Furthermore, the study revealed that the minimum fluid flow rate is sufficient to attain the maximum enhancement in heat transfer rate.

### **Acknowledgment**

The authors are grateful for the management of the Kongu Engineering College and Department of Chemical Engineering for the facility provided.

## Nomenclature

$\text{Al}_2\text{O}_3$	Aluminium Oxide
$\text{TiO}_2$	Titanium dioxide
$\text{ZnO}$	Zinc Oxide
$\text{Fe}_2\text{O}_3$	Iron Oxide
$\text{CuO}$	Copper Oxide
$\text{SiO}_2$	Silicon dioxide
CNT	Carbon Nano Tubes
D	Dimension
$D_H$	Hydraulic diameter, m
$\Delta T_{\text{LMTD}}$	Logarithmic Mean Temperature Difference
T	Therminol-55
G	Glycerol
W	Water
m	Mass, kg
U	Overall Heat transfer coefficient, $\text{W}/\text{m}^2 \cdot \text{K}$
$N_{\text{Nu}}$	Nusselt number, dimensionless
$N_{\text{Pr}}$	Prandtl Number, dimensionless
$N_{\text{Re}}$	Reynolds number, dimensionless
Q	Heat Flux, W
$C_p$	Specific heat capacity, $\text{J}/(\text{kg} \cdot \text{K})$
PHE	Plate Heat Exchanger
Pr	Prandtl number, dimensionless
H	Heat transfer coefficient, $\text{W}/\text{m}^2 \cdot \text{K}$
$H_h$	Hot Fluid Heat transfer coefficient, $\text{W}/\text{m}^2 \cdot \text{K}$
$H_c$	Cold Fluid Heat transfer coefficient, $\text{W}/\text{m}^2 \cdot \text{K}$
vol. %	Volume %
Greek symbols	
$\beta$	corrugation angle, °
$\rho$	density, $\text{kg}/\text{m}^3$

$\mu$	dynamic viscosity, Pa s
$\phi$	nanoparticle volume fraction, dimensionless
$k$	thermal conductivity, W/ (m.K)
$\Pi$	Corrugation angle

## References

1. S.U.S. Choi, S. Lee, S. Li, J.A. Eastman, J. Heat Transfer 121 (1999) 280-289.  
<https://doi.org/10.1115/1.2825978>.
2. S.K. Das, N. Putra, P. Thiesen, W. Roetzel, J. Heat Transfer 125 (2003) 567-574.  
<https://doi.org/10.1115/1.1571080>.
3. S.S. Sonawane, R. S., Khedkar, K.L.T. Wasewar, Int. Commun. Heat Mass Transfer 49 (2013) 60-68. <https://doi.org/10.1016/j.icheatmasstransfer.2013.10.001>.
4. M.A. Sabiha, R. Saidur, S. Mekhilef, O. Mahian, Renewable Sustainable Energy Rev. 51 (2015) 1038-1054. <https://doi.org/10.1016/j.rser.2015.07.016>.
5. S.P. Manikandan, N. Dharmakkan, S. Nagamani, Chem. Ind. Chem. Eng. Q. 28 (2022) 95-101. <https://doi.org/10.2298/CICEQ210125021M>
6. S.P. Manikandan, N. Dharmakkan, M.D. Sri Vishnu, H. Prasath, R. Gokul, Hem. Ind. 75 (2021) 341-352. <https://doi.org/10.2298/HEMIND210520031S>.
7. S.P. Manikandan, N. Dharmakkan, M.D. Sri Vishnu, H. Prasath, R. Gokul, G. Thiagarajan, G. Sivasubramani, B. Moulidharan, Chem. Ind. Chem. Eng. Q. 29 (2023) 225-233. <https://doi.org/10.2298/CICEQ220430029S>
8. M.M. Sarafraz, A.D. Baghi, M.R. Safaei, A.S. Leon, R. Ghomashchi, M. Goodarzi, C.X. Lin, Energies 12 (2019) 1-13. <https://doi.org/10.3390/en12224327>
9. W. Xu, S. Wang, Q. Zhang, Q., Wang, H. Lu, H. Tan, Appl. Therm. Eng. 95 (2016) 165-177. <https://doi.org/10.1016/j.applthermaleng.2015.10.164>.
10. E. Abu-Nada, Int. J. Heat Fluid Flow 30 (2009) 489-500.  
<https://doi.org/10.1016/j.ijheatfluidflow.2009.02.003>
11. M.M. Sarafraz, A.D. Baghi, M.R. Safaei, A.S. Leon, R. Ghomashchi, M. Goodarzi, C.X. Lin, Energies 12 (2019) 1-13. <https://doi.org/10.3390/en12224327>

12. S.P. Manikandan, R. Baskar, Chem. Ind. Chem. Eng. Q. 27 (2021) 15-20.  
<https://doi.org/10.2298/CICEQ191220020P>.
13. B. Sahin, E. Manay, E.F. Akyurek, J. Nanomater. 2015 (2015) 1-10.  
<https://doi.org/10.1155/2015/790839>
14. S. Hoseinzadeh, P.S. Heyns, H. Kariman, Int. J. Numer. Methods Heat Fluid Flow 30 (2020) 1149–116. <https://doi.org/10.1108/HFF-06-2019-0485>.
15. S.P. Manikandan, P.K. Chinnusamy, R. Thangamani, S. Palaniraj, P. Ravichandran, S. Karuppasamy, Y.R. Sanmugam, Chem. Ind. Chem. Eng. Q. 30 (2024) 257-264.  
<https://doi.org/10.2298/CICEQ230726028M>
16. S.P. Manikandan, R. Baskar, Chem. Ind. Chem. Eng. Q. 27 (2021) 177-187.  
<https://doi.org/10.2298/CICEQ200504036P>
17. S.P. Manikandan, R. Baskar, Chem. Ind. Chem. Eng. Q. 24 (2018) 309-318.  
<https://doi.org/10.2298/CICEQ170720003M>.
18. S.P. Manikandan, R. Baskar, Period. Polytech., Chem. Eng. 62 (2018) 317-322.  
<https://doi.org/10.3311/PPch.11676>
19. T. Maré, S. Halelfadl, O. Sow, P. Estellé, S. Duret, F. Bazantay, Exp. Therm. Fluid Sci. 35 (2011) 1535-1543. <https://doi.org/10.1016/j.expthermflusci.2011.07.004>.
20. A. Munimathan, T. Sathish, V. Mohanavel, A. Karthick, R. Madavan, R. Subbiah, S. Rajkumar, Int. J. Photoenergy 1 (2021) 6680627. <https://doi.org/10.1155/2021/6680627>.
21. M. M. Sarafraz, A. Dareh Baghi, M. R. Safaei, A.S. Leon, R. Ghomashchi, M. Goodarzi, C. Lin, Energies 12 (2019) 4327. <https://doi.org/10.3390/en12224327>.
22. A. M. Hassaan, Heat Trans. Res. 53 (2022) 19 - 34.  
<https://doi.org/10.1615/HeatTransRes.2022042147>
23. A. M. Hassaan, Int. J. Therm. Sci. 177 (2022) 107569.  
<https://doi.org/10.1016/j.ijthermalsci.2022.107569>

24. A. M. Hassaan, Heat Trans. Res. 54 (2023) 1 - 16.  
<https://doi.org/10.1615/HeatTransRes.2023045768>
25. A. M. Hassaan, Proc. Inst. Mech. Eng., Part E 236 (2022) 2139-2146.  
<https://doi.org/10.1177/09544089221086825>
26. A. M. Hassaan, Proc. Inst. Mech. Eng., Part E 237 (2022) 1310-1318.  
<https://doi.org/10.1177/09544089221113977>
27. A. M. Hassaan, Heat Mass Transfer 60 (2024) 1211-1219.  
<https://doi.org/10.1007/s00231-024-03487-8>
28. M. M. Sarafraz, A. Dareh Baghi, M. R. Safaei, A.S. Leon, R. Ghomashchi, M. Goodarzi, C. Lin, Energies 12 (2019) 4327. <https://doi.org/10.3390/en12224327>.
29. N. S. Sahid, M.M. Rahman, K. Kadirgama, M.A. Maleque, J. Mech. Eng. Sci. 11 (2017) 3087- 3094. <https://doi.org/10.15282/jmes.11.4.2017.11.0277>
30. B. Barbés, R. Páramo, E. Blanco, M.J. Pastoriza-Gallego, M.M. Pineiro, J.L. Legido, C.J. Casanova, J. Therm. Anal. Calorim. 111 (2013) 1615- 1625.  
<https://doi.org/10.1007/s10973-012-2534-9>
31. S.Z. Heris, T.H. Nassan, S.H. Noie, H. Sardarabadi, M. Sardarabadi, Int. J. Heat Fluid Flow 44 (2013) 375 – 382. <https://doi.org/10.1016/j.ijheatfluidflow.2013.07.006>.
32. B. Mehta, D. Subhedar, Mater. Today: Proc. (2023).  
<https://doi.org/10.1016/j.matpr.2023.09.142>
33. M. A. Rahman, S. M. Hasnain, S. Pandey, A., Tapalova, N., Akylbekov, R. Zairov, ACS omega 9 (2024) 32328-32349. <https://doi.org/10.1021/acsomega.4c03279>
34. M. M. Arani, Micro and Nano Technologies (2024) 45 - 75.  
<https://doi.org/10.1016/B978-0-443-13625-2.00003-6>
35. R.S. Khedkar, A. Saikiram, S.S. Sonawane, K. Wasewar, S.S. Umre, Procedia Eng. 51 (2013) 342-346. <https://doi.org/10.1016/j.proeng.2013.01.047>
36. W. Yu, H. Xie, L. Chen, Y. Li, Colloids Surf., A 355 (2010) 109-113. .  
<https://doi.org/10.1016/j.colsurfa.2009.11.044>

### **Figure Captions**

Figure 1: SEM image of Al<sub>2</sub>O<sub>3</sub> nanoparticle

Figure 2: Schematic and Photographic view of the experimental set up

Figure 3: Effect of flow rate on hot fluid heat transfer coefficient ( $h_h$ ) for Therminol-55/Water base fluid at 60°C

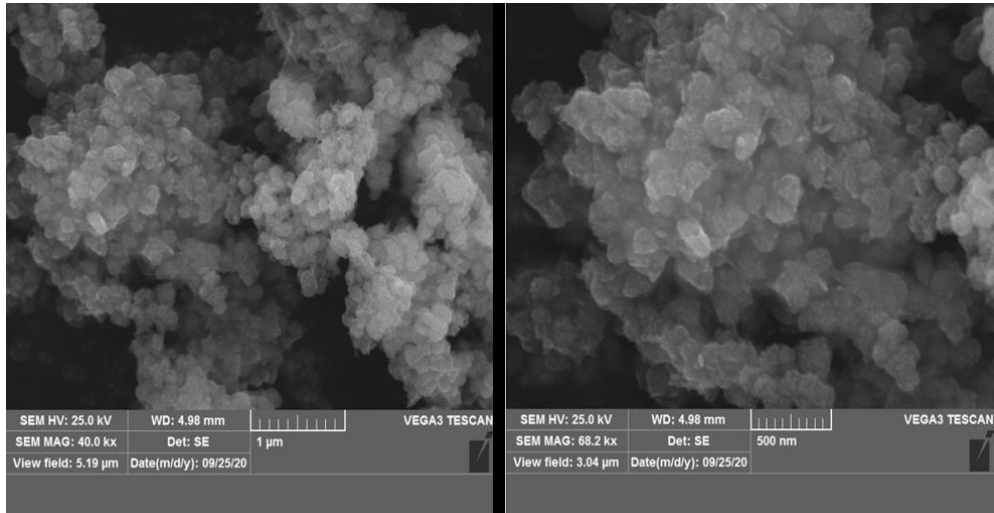
Figure 4: Effect of flow rate on cold fluid heat transfer coefficient ( $h_c$ ) for Therminol-55/Water base fluid at 60°C

Figure 5: Effect of flow rate on hot fluid heat transfer coefficient ( $h_h$ ) for Glycerol/Water base fluid at 60°C

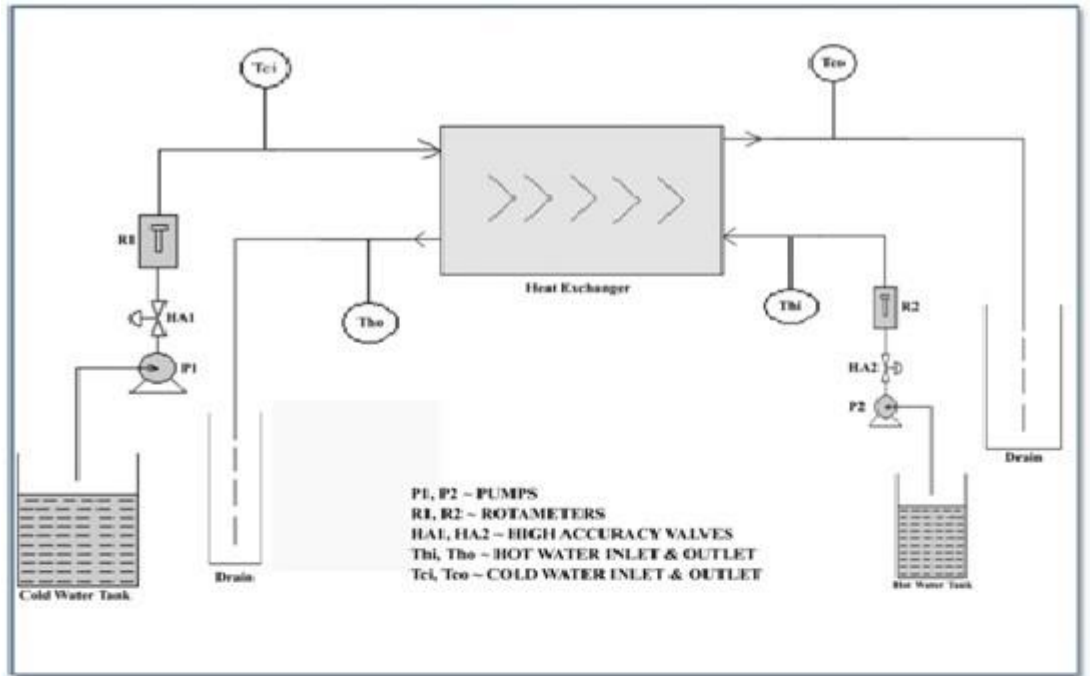
Figure 6: Effect of flow rate on cold fluid heat transfer coefficient ( $h_c$ ) for Glycerol/Water base fluid at 60°C

Figure 7: Effect of flow rate on overall heat transfer coefficient (U) for Therminol-55/Water and Glycerol/Water base fluid at 60°C

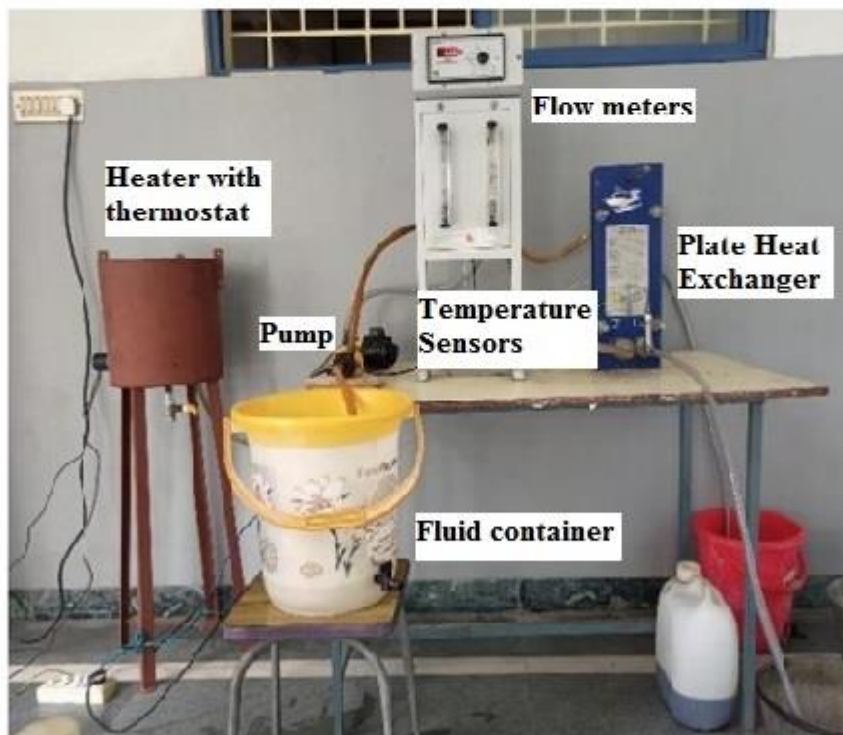




**Figure 1**



(a) Schematic diagram



(b) Photographic view

Figure 2

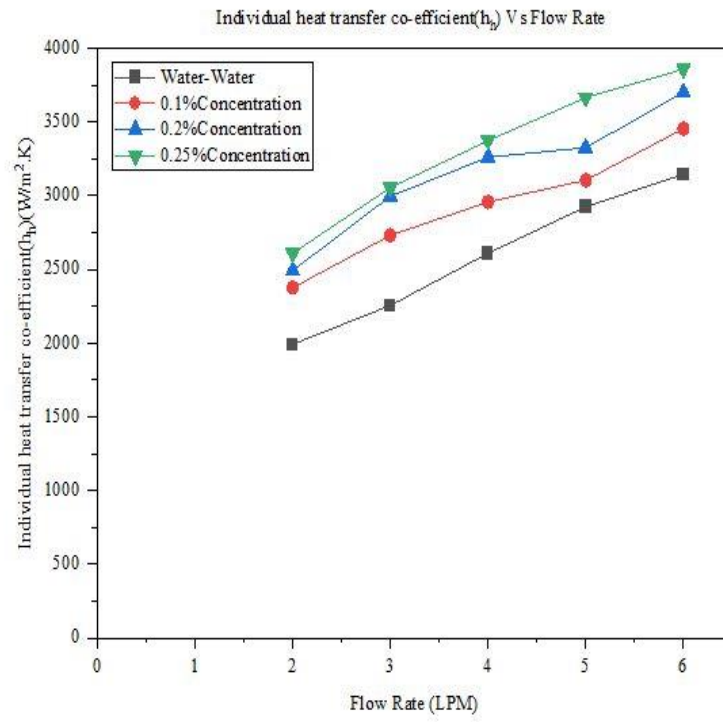


**Figure 3**

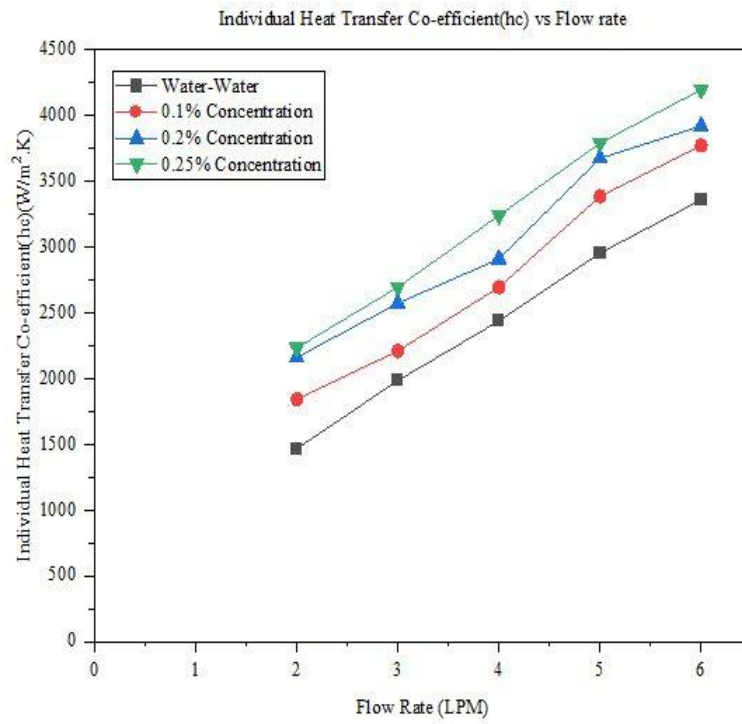


**Figure 4**

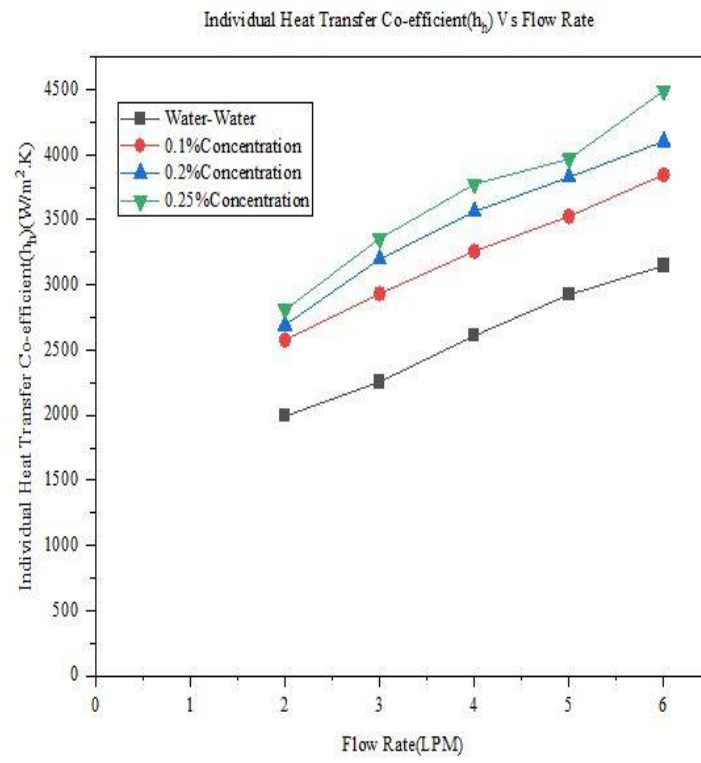


**Figure 5**

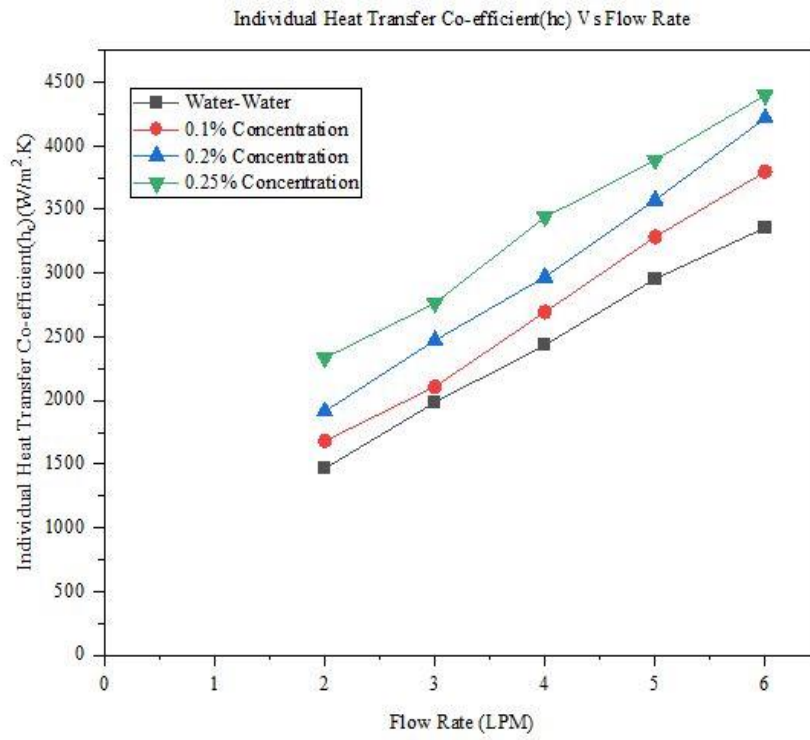


**Figure 6**

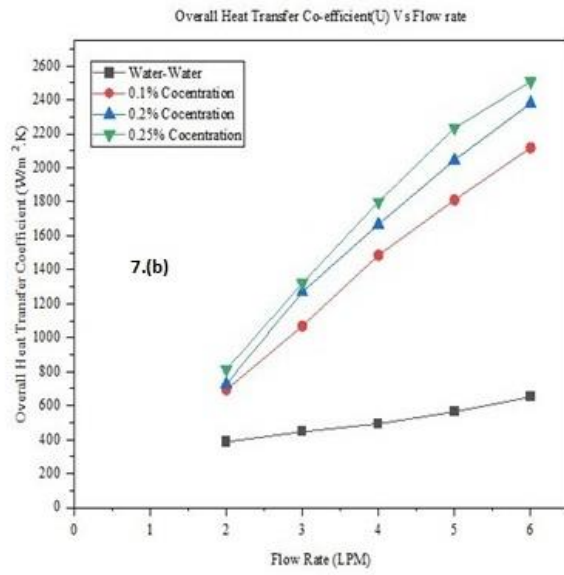
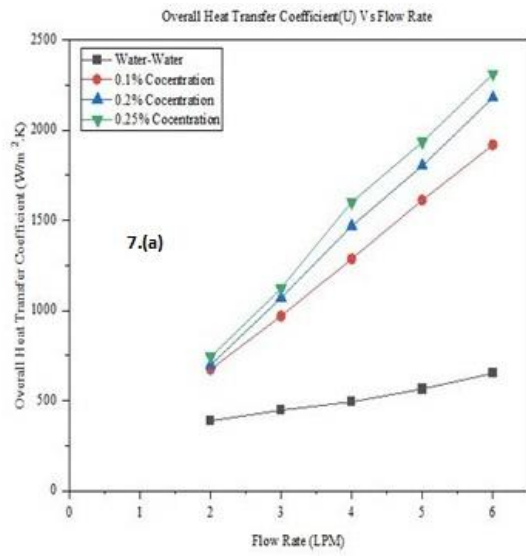


Figure 7